Deterministic Equations for Feedback Control of Open Quantum Systems

Alberto J. B. Rosal,[1,2,*] Patrick P. Potts,[3] and Gabriel T. Landi[1,2]

[1]*Department of Physics and Astronomy, University of Rochester, Rochester, New York 14627, USA*
[2]*University of Rochester Center for Coherence and Quantum Science, Rochester, New York 14627, USA*
[3]*Department of Physics and Swiss Nanoscience Institute, University of Basel, Klingelbergstrasse 82 CH-4056, Switzerland*

(Received 11 August 2025; accepted 25 June 2026; published 28 July 2026)

Feedback control in open quantum dynamics is crucial for the advancement of various coherent platforms. However, currently only a handful of feedback master equations exist in the literature, which are restricted to specific types of feedback. In this letter we first introduce a unifying framework, based on a single general equation, that describes all possible feedback schemes in sequentially (and continuously) measured systems, and from which all previous results follow. Next, we specialize it to the case of quantum jumps and introduce a new type of feedback based on the channel of the last detected jump, as well as the time elapsed since it occurred. Our description is experimentally grounded, and naturally allows for the introduction of realistic effects, such as time-delays in the feedback loop. We illustrate our results with two time-dependent feedback protocols conditioned on quantum-jump detections: one achieving population inversion of a two-level system against a thermal bath, and another enabling real-time reversal of quantum transitions, both admitting steady-state solutions.

DOI: 10.1103/pg2p-h529

Introduction—Feedback refers to the process of dynamically controlling a system based on previous detection outcomes (see Fig. 1). It plays a central role across quantum coherent platforms, including cooling protocols [1–10], quantum error correction [11,12], entanglement generation [13], thermodynamics [14–16], transport [17], control [18–20], and quantum batteries [21]. It has enabled experimental realizations of Maxwell's demon in the quantum regime [22–24], motivating generalized formulations of the second law that incorporate feedback [25–27] and underscoring its importance in both theory and experiment.

The theoretical description of feedback in open quantum systems is nontrivial. Only a limited set of feedback master equations has been derived [11,28–32], typically restricted to specific measurements and feedback schemes. For example, Ref. [29] considers weak Gaussian measurements [33] with low-pass filtering, while Ref. [30] employs feedback based on homodyne outcomes. Consequently, realistic feedback protocols often rely on stochastic differential equations [34–41], which are noisy, computationally demanding, and lacking in physical insights. In contrast, feedback master equations often yield analytical results valid across broad parameter ranges, revealing parameter dependencies and universal features.

The lack of feedback equations is dire for protocols based on quantum jumps, which are central to many experiments, from optical cavities [42,43] to quantum dots [44,45], where jumps can be detected in real time. One of the few available results is Ref. [31], which implements the following protocol: upon detection of a quantum jump, an instantaneous quantum channel (e.g., a pulse) is applied. However, this framework does not capture many relevant scenarios, such as applying a coherent drive for a finite duration or transiently modifying system parameters after a jump. These protocols have been implemented in quantum-dot experiments, where jumps are monitored via a quantum point contact [44,45], although a corresponding feedback equation is still unavailable [46].

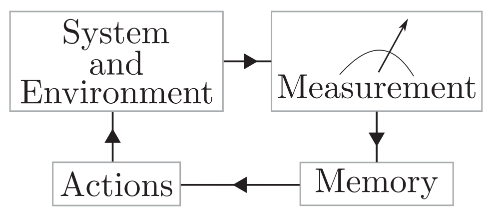

FIG. 1. General feedback diagram. A detection outcome is stored in memory and used in a feedback action that can modify the system dynamics (e.g., the Hamiltonian H), the environment (e.g., bath temperature), or the measurement process itself.

In this Letter, we fill this gap by introducing a general framework for sequential feedback protocols that provides analytical treatments in previously inaccessible regimes, all derived from a single equation (Result 1). In Supplemental Material [48], we recover all previously known feedback equations as special cases of Result 1. As our second main result, we specialize this framework to quantum jumps and derive a new class of feedback that is based on both the channel of the last jump, as well as the time elapsed since

[*]Contact author: abezerra@ur.rochester.edu

the last jump (Result 2). This is motivated by recent experiments, such as in quantum dot devices.

We apply our framework to two time-dependent feedback protocols conditioned on quantum-jump detections: (i) population inversion of a qubit coupled to a thermal bath, and (ii) real-time reversal of quantum transitions. These experimentally relevant schemes [42–45] lie beyond the scope of previous deterministic feedback formulations [29–32]. Further developments and applications of this framework are presented in follow-up works [49,50].

Memory and data processing—Feedback can be described in terms of the diagram in Fig. 1. A system is sequentially measured, yielding a string of random outcomes $(x_1, x_2, \ldots, x_n, \ldots)$, where x_i is the outcome at the discrete time t_i (the continuous-time version can be obtained as a limit [51]). The feedback protocol consists of a set of possible actions, which can be applied to the system, and which are chosen based on the observed data. This could be, e.g., applying a laser drive, or changing a gate voltage. The key aspects that define the protocol are (i) the type of measurement (projective, diffusive, quantum jumps, etc.); and (ii) what data is actually being used to construct the feedback actions. The latter is particularly nontrivial. At step n, the data available is in principle the full set $x_{1:n} \equiv (x_1, x_2, \ldots, x_n)$, but not all of it might actually be needed.

A general approach stores part or all of the past measurement record in a memory, denoted here by y_n. Hence, the memory is a function of the previous outcomes, $y_n = y_n(x_{1:n})$, and may represent either the full dataset, $y_n = (x_1, x_2, \ldots, x_n)$, or a compressed version of it. Adding a memory requires an additional data processing step, where the new value y_n is updated according to some function $y_n = f_n(x_n, y_{n-1})$, that depends on the latest outcome x_n, as well as the past memory value y_{n-1}. With an appropriate choice of data-processing function f_n, one can describe all possible feedback schemes.

For instance, the simplest feedback scheme uses only the latest outcome x_n [30,31], with the data-processing function $f_n(x_n, y_{n-1}) = x_n$, corresponding to a compression that discards all previous outcomes. At the opposite extreme, one may retain the entire record $(x_1, \ldots, x_n)$ using $f_n(x_n, y_{n-1}) = \mathrm{append}(y_{n-1}, x_n)$, where each new outcome is appended to the memory, and no compression is applied. Furthermore, feedback schemes can depend on summary statistics of the record $(x_1, \ldots, x_n)$, such as the sample mean [32], $y_n = (x_1 + \cdots + x_n)/n$, with the update function $f_n(x_n, y_{n-1}) = (x_n + (n-1)y_{n-1})/n$. Additional examples of data-processing functions are given in [48].

Sequential measurements—A general description of sequentially measured systems is given in terms of *instruments* $\{\mathcal{M}_x\}$, i.e., trace nonincreasing maps associated with outcome x, such that $\sum_x \mathcal{M}_x$ defines a quantum channel [52]. For a state ρ, the probability of outcome x is $\mathrm{Tr}(\mathcal{M}_x\rho)$, and the postdetection state is $\mathcal{M}_x\rho/\mathrm{Tr}(\mathcal{M}_x\rho)$.

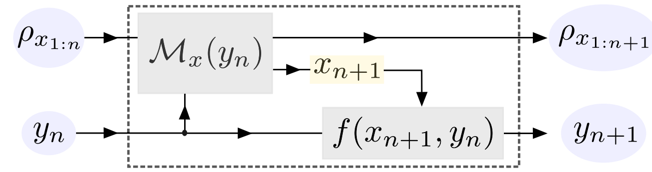

FIG. 2. Conditional evolution under feedback. The instruments $\mathcal{M}_x$ describe both the system dynamics and the measurement process at each step. The quantities $\rho_{x_{1:n}}$ and y_n denote, respectively, the system state and memory after n detections given the dataset $(x_1, \ldots, x_n)$. Feedback is implemented by using the memory y_n to modify the instrument, while the measurement yields the outcome x_{n+1} and updates the memory as $y_{n+1} = f(x_{n+1}, y_n)$.

Instruments capture both the system dynamics and the measurement process, providing a unified framework for phenomena ranging from projective measurements to quantum jump detections. For example, consider a system measured at regular intervals $\delta t > 0$ with Kraus operators $\{V_x\}$, and intermediate dynamic evolution given by $\rho(t+\delta t) = \Lambda_{\delta t}\rho(t)$. The corresponding instrument is $\mathcal{M}_x\rho = V_x[\Lambda_{\delta t}(\rho)]V_x^\dagger$.

The most general feedback mechanism consists of dynamically modifying the instrument $\mathcal{M}_{x_{n+1}}$ at each time step t_{n+1}, based on the memory y_n stored at that step (see Fig. 2). The stochastic dynamics in the presence of feedback is therefore described by the following rules

$$P(x_{n+1}|x_{1:n}) = \mathrm{Tr}[\mathcal{M}_{x_{n+1}}(y_n)\rho_{x_{1:n}}],$$
$$\rho_{x_{1:n+1}} = \frac{\mathcal{M}_{x_{n+1}}(y_n)\rho_{x_{1:n}}}{P(x_{n+1}|x_{1:n})}, \tag{1}$$

where $\rho_{x_{1:n}}$ denotes the state conditioned on the dataset $x_{1:n}$.

Our goal is to derive a deterministic equation governing the time evolution of a general feedback protocol. To do that we define the memory-resolved state [29,32] (also called hybrid state [28,53–56]) as $\varrho_n(y) = E[\rho_{x_{1:n}}\delta_{y,y_n}]$, where $E[\cdot]$ denotes the average over trajectories, and δ_{y,y_n} is the Kronecker delta. The trace of this state gives the distribution of the memory function y_n, $\mathrm{Tr}[\varrho_n(y)] = P(y_n = y)$, while the marginalization over all realizations of y_n yields the unconditional state of the system, $\sum_y \varrho_n(y) = \bar{\rho}_n$. Notice that $\rho_{x_{1:n}}$ is a stochastic (conditional) state, but $\varrho_n(y)$ is deterministic. Our first main result is:

Result 1—If an instrument $\{\mathcal{M}_x(y)\}$ depends only on a causal memory function $y_n = f_n(x_n, y_{n-1})$, the corresponding memory-resolved state $\varrho_n(y)$ evolves according to the deterministic equation

$$\varrho_{n+1}(y) = \sum_{x',y'} \delta_{y,f_{n+1}(x',y')}\mathcal{M}_{x'}(y')\varrho_n(y'), \tag{2}$$

where the sum runs over all possible outcomes x' and all possible realizations y' of y_n.

The proof can be found in [48]. Since $\varrho_n(y)$ is resolved in y, the state at step $n+1$ should be just a sum over all possible trajectories consistent with the constraint $y_n = f_n(x_n, y_{n-1})$. Result 1 provides a single, general equation for any feedback scheme in sequentially measured systems, and all previously known feedback equations [29–32] are recovered as special cases [48]. In the remainder of the paper, we employ this framework to derive a new class of feedback strategies based on quantum jump detections.

Quantum jumps—We consider a system that is described by the quantum master equation

$$\partial_t \rho_t = \mathcal{L}\rho = -i[H, \rho_t] + \sum_k L_k \rho_t L_k^\dagger - \frac{1}{2}\{L_k^\dagger L_k, \rho_t\}, \quad (3)$$

with Hamiltonian H and jump operators L_k. We assume that there is a subset of quantum jumps $k \in \Sigma$, which can be experimentally monitored. Within the quantum jump unravelling, this means that the dynamics for an infinitesimal step δt can be decomposed into a set of instruments [57]

$$\mathcal{M}_0 \rho = (1 + \delta t \mathcal{L}_0)\rho, \quad (4)$$

$$\mathcal{M}_k \rho = \delta t \mathcal{J}_k \rho, \quad (5)$$

where $\mathcal{J}_k \rho = L_k \rho L_k^\dagger$, $\mathcal{L}_0 = \mathcal{L} - \sum_{k\in\Sigma} \mathcal{J}_k$. At the stochastic level, the outcome at step $t_n = n\delta t$ is either $x_n = 0$ (no jump) or $x_n = k$ for a jump of type k. Our goal is to introduce feedback schemes that allow for both the Hamiltonian H, and the jump operators, to be modified in real time based on these measurements.

We consider two types of memories. First, one that records the channel $k \in \Sigma$ of the last jump. This can be constructed with a function f_n of the form

$$k_n = x_n + k_{n-1}\delta_{x_n,0}. \quad (6)$$

Second, a memory that records how much time has elapsed since the last jump, which is built using

$$\tau_n = \delta_{x_n,0}(\tau_{n-1} + \delta t). \quad (7)$$

We refer to them as the jump and counting memories, respectively. A general feedback mechanism based on both jump and counting memories is defined by the total memory function $y_n = (k_n, \tau_n)$, with the instruments given in Eqs. (4) and (5). In this setting, the feedback allows both the system Hamiltonian and the jump operators at time t_{n+1} to depend on the last detected jump k_n and the elapsed time τ_n, taking the forms $H(k_n, \tau_n)$ and $L_k(k_n, \tau_n)$, which in turn define the corresponding superoperators $\mathcal{L}_0(k_n, \tau_n)$ and $\mathcal{J}_k(k_n, \tau_n)$. Starting from Result 1, we show in [48] the following result:

Result 2—Let $\varrho_t(k, \tau)$ denote the state of the system resolved in both the jump and counting memory functions (6), (7). In the limit $\delta t \to 0$ this evolves according to the deterministic equations

$$\varrho_t(k, 0) = 2\delta(t)\delta_{k,\bar{k}}\bar{\rho}_0 + \sum_{q\in\Sigma}\int_0^t d\tau\, \mathcal{J}_k(q, \tau)\varrho_t(q, \tau), \quad (8)$$

$$\varrho_t(k, \tau) = G(k, \tau)\varrho_{t-\tau}(k, 0), \quad (9)$$

where $G(k, \tau) \equiv \mathcal{T}[e^{\int_0^\tau ds \mathcal{L}_0(k,s)}]$ is the propagator of the no-jump evolution and $\mathcal{T}[\cdot]$ is the time-ordering operator.

In the limit $\delta t \to 0$, the memory functions defined in Eqs. (6) and (7) become continuous-time stochastic processes, k_t and τ_t, specifying that at time t the last jump occurred in channel k_t at time $t - \tau_t$. The quantity $\mathrm{Tr}[\varrho_t(k, \tau)]$ is the joint distribution of (k_t, τ_t), and from (7) it follows that $\tau_t \in [0, t]$. The resolved state is normalized as $\sum_{k\in\Sigma}\int_0^t \mathrm{Tr}[\varrho_t(k, \tau)]d\tau = 1$, and the unconditional state is recovered as

$$\bar{\rho}_t = \sum_{k\in\Sigma}\int_0^t d\tau\, \varrho_t(k, \tau). \quad (10)$$

The term $2\delta(t)\delta_{k,\bar{k}}\bar{\rho}_0$ encodes the initial condition, with system state $\bar{\rho}_0$ and memory values $k_0 = \bar{k}$ and $\tau_0 = 0$. We adopt the convention $\int_0^t d\tau\, \delta(t - \tau) = 1/2$. Result 2 enables time-dependent control actions, such as temporarily modifying the system Hamiltonian or environmental parameters. In contrast, previous jump-based schemes [31] relied solely on the current jump detection. Although Result 2 cannot, in general, be expressed as a differential equation, it remains amenable to analytical treatment—as detailed in [48]—especially in the stationary regime.

Let us consider the special case where the feedback depends only on the last detected jump recorded by k_t, regardless of the time elapsed since its detection. We show in [48] that the marginal state $\varrho_t(k) = \int_0^t d\tau\, \varrho_t(k, \tau)$ will evolve as

$$\partial_t \varrho_t(k) = -i[H(k), \varrho_t(k)] - \frac{1}{2}\sum_{k'\in\Sigma}\{L_{k'}^\dagger(k)L_{k'}(k), \varrho_t(k)\} + \sum_{k'\in\Sigma} L_k(k')\varrho_t(k')L_k^\dagger(k'). \quad (11)$$

Equation (11) represents a system of coupled equations, one for each jump channel $k \in \Sigma$, describing protocols that update the Hamiltonian and/or jump operators based on k_t. A similar equation was derived in [58] in a different context.

Returning to the general Result 2, the situation simplifies when the feedback is applied only on the no-jump part of the dynamics (e.g., in the Hamiltonian). In this case $\mathcal{J}_k(k', \tau') = \mathcal{J}_k$ and Eqs. (8)–(10) imply that $\varrho_t(k,\tau) = 2\delta(t-\tau)\delta_{k,\bar{k}}G(k,\tau)\bar{\rho}_0 + G(k,\tau)\mathcal{J}_k\bar{\rho}_{t-\tau}$. The memory-resolved state can hence be written in terms of the unconditional state $\bar{\rho}_t$ which, in turn, satisfies the closed integral equation

$$\bar{\rho}_t = G(\bar{k}, t)\bar{\rho}_0 + \sum_{k\in\Sigma}\int_0^t d\tau G(k,\tau)\mathcal{J}_k\bar{\rho}_{t-\tau}. \quad (12)$$

The steady state, if it exists, is obtained by setting $t \to \infty$. In this case, $\lim_{t\to\infty} G(k,t) = 0$ [48], so $\bar{\rho}_{\rm ss}$ will therefore be the solution of the algebraic equation

$$\bar{\rho}_{\rm ss} = \Omega\bar{\rho}_{\rm ss}, \qquad \Omega = \sum_{k\in\Sigma}\int_0^\infty d\tau G(k,\tau)\mathcal{J}_k, \quad (13)$$

which also provides the steady-state memory-resolved state $\varrho_{\rm ss}(k,\tau) = G(k,\tau)\mathcal{J}_k\bar{\rho}_{\rm ss}$. In turn, this can be used to calculate various time-related properties, such as waiting-time distributions, the average time between jumps, etc. The ability to describe jump statistics under a general feedback protocol, as given by $\mathrm{Tr}[\varrho_t(k,\tau)]$, is a novel feature not captured by any previous feedback formulation.

Example 1: Inversion protocol—Two-level systems (qubits) in excited states act as single-photon sources of nonclassical light [59] and as key elements in quantum computing [60]. Coupled to a thermal bath, they relax to a steady state with a higher ground-state population than excited-state population ($P_g > P_e$). Our goal is to achieve population inversion ($P_g < P_e$) via time-dependent feedback and continuous monitoring of quantum jumps. Let $|e\rangle$ and $|g\rangle$ denote the excited and ground states with energy gap ω. The thermal reservoir has temperature T, and the jump operators are $L_- = \sqrt{\gamma(\bar{N}+1)}|g\rangle\langle e|$ and $L_+ = \sqrt{\gamma\bar{N}}|e\rangle\langle g|$ describing, respectively, the emission and absorption of a quanta, where $\gamma > 0$ is the coupling strength, and $\bar{N} = (\exp(\omega/T) - 1)^{-1}$.

The protocol is defined as follows [see Fig. 3(a)]. In the rotating frame at frequency ω_d, the qubit Hamiltonian reads $H = -(\Delta/2)\sigma_z$, where $\sigma_{x,y,z}$ are the Pauli matrices and $\Delta \equiv \omega - \omega_d$ (see Ref. [48] for technical details). Upon detecting a thermal emission ($|e\rangle \to |g\rangle$) and observing no subsequent detection for a time τ_0, an external drive with amplitude λ and frequency ω_d is applied for a duration τ_1, and the Hamiltonian becomes $H = -(\Delta/2)\sigma_z + \lambda\sigma_x$. In essence, after an emission and a time τ_0, the drive induces Rabi oscillations for a time τ_1, transferring population from $|g\rangle$ back to $|e\rangle$.

This protocol is described by Result 2, as it depends on both the last detected jump and the elapsed time. The End Matter provides analytical steady-state results, including the optimal drive duration $\tau_1^{\rm opt}$ [Eq. (A1)] that maximizes the excited-state population. Notably, $\tau_1^{\rm opt}$ generally differs from a π pulse, as dissipation requires a longer drive,

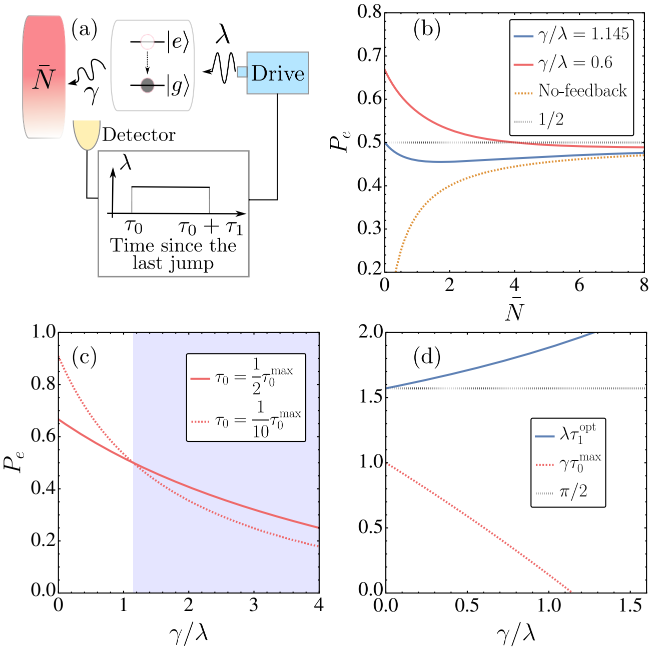

FIG. 3. Population inversion via time-dependent feedback with quantum jumps. (a) Upon detection of a decay event, an external drive is applied to return the qubit to the excited state. (b) Population of the excited state without feedback delay ($\tau_0 = 0$), and considering the optimal drive duration $\tau_1^{\rm opt}$ [Eq. (A1)]. The no-feedback line corresponds to a qubit coupled to a thermal bath without an external drive. (c) Effect of feedback delay on the excited-state population for $\bar{N} = 0$. (d) Maximum allowable feedback delay and the optimal drive duration for $\bar{N} = 0$.

highlighting the interplay between coherence and dissipation in the feedback dynamics. Determining this optimal time from stochastic simulations would be cumbersome due to the large parameter space. Figure 3(b) shows P_e as a function of $\bar{N}$ for the ideal case without time delay ($\tau_0 = 0$) and considering the optimal drive duration $\tau_1^{\rm opt}$. We find that for $\gamma/\lambda \leq 1.145$, there exists a critical value $\bar{N}_{\rm c} \geq 0$ such that $P_e > 1/2$ for all $\bar{N} < \bar{N}_{\rm c}$. This therefore establishes the population inversion threshold. In Fig. 3(c), we illustrate how P_e is affected by varying the delay τ_0 for $\bar{N} = 0$ [Eq. (A2)], demonstrating how increasing τ_0 deteriorates the population inversion.

Figure 3(d) shows the optimal drive duration $\tau_1^{\rm opt}$ [Eq. (A1)] and the maximum delay $\tau_0^{\rm max}$ [Eq. (A3)] enabling population inversion for $\bar{N} = 0$. In the strong-drive regime ($\gamma \ll \lambda$), we find that $\tau_0^{\rm max} \sim 1/\gamma$, indicating that the maximum delay is on the order of the system's natural timescale γ^{-1}. Conversely, $\tau_0^{\rm max} = 0$ for $\gamma/\lambda > 1.145$, reflecting that population inversion is no longer possible in this regime, regardless of the feedback delay. Additionally, we observe that $\gamma\tau_1^{\rm opt}$ increases with γ/λ, implying that as the drive strength λ decreases relative to γ, the drive must remain on for a longer duration to

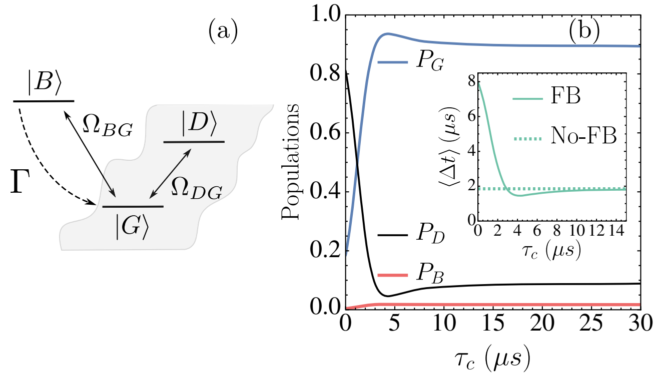

FIG. 4. Reverting quantum transitions. (a) Three-level system with a hidden transition [43] between the ground $|G\rangle$ and dark $|D\rangle$ states (shaded region). The states $|B\rangle$ and $|G\rangle$ are coupled to an effective thermal bath, analogous to the qubit setup in Example 1, with coupling rate γ_B and Bose–Einstein occupation $\bar{N}_B$, so that $\Gamma = \gamma_B(\bar{N}_B + 1)$. The protected states $|D\rangle$ and $|G\rangle$ are only weakly coupled to a second bath characterized by γ_D and $\bar{N}_D$. (b) Populations of the feedback steady state as a function of the waiting time τ_c. The inset shows the average time $\langle\Delta t\rangle$ between jumps $|B\rangle \to |G\rangle$ in the stationary regime. The limit $\tau_c \to \infty$ corresponds to the no-feedback case, where no rotations are applied. Parameters: $\Omega_{BG}/(2\pi) = 0.9$ MHz, $\gamma_B = 10\Omega_{BG}$, $\Omega_{DG}/(2\pi) = 14$ kHz, $\gamma_D = 0.875\Omega_{DG}$, $\bar{N}_B = 0.01$, $\bar{N}_D = 0.05$, $\theta = \phi = \pi/2$.

optimize P_e. On the other hand, when dissipation is weak ($\gamma \ll \lambda$), the optimal drive duration recovers the π pulse.

Example 2: Reverting quantum transitions—Reference [43] showed that quantum transitions can be continuously monitored and reversed in real time via feedback. There, upon detecting the beginning of a transition, a pulse is applied after a time τ_c to reverse its evolution, originally described using stochastic simulations. We apply our formalism to this setup with photon-counting detection [61–64]. Rather than averaging many trajectories, our method yields the steady state from a single eigenvector equation and directly provides stationary jump statistics, including the mean interjump time.

The system [Fig. 4(a)] consists of a ground state $|G\rangle$, a protected (dark) state $|D\rangle$ designed to minimally couple to any dissipative environment or measurement apparatus, and a bright state $|B\rangle$ that decays incoherently to $|G\rangle$ with coupling rate Γ, emitting a photon. A weak Rabi drive Ω_{DG} couples $|G\rangle$ and $|D\rangle$, while a stronger drive Ω_{BG} satisfies $\Omega_{DG} \ll \Omega_{BG} \ll \Gamma$, linking the populations of $|G\rangle$ and $|B\rangle$. The incoherent jump $|B\rangle \to |G\rangle$ is monitored by detecting the emitted photon, which signals occupation of $|G\rangle$, while a prolonged absence of photons indicates coherent evolution within the $\{|G\rangle, |D\rangle\}$ subspace. The protocol proceeds as follows: after detecting the incoherent jump $|B\rangle \to |G\rangle$ and observing no further detection for a time τ_c, a pulse is applied on the $\{|G\rangle, |D\rangle\}$ Bloch sphere, corresponding to a rotation by angle θ around the axis $\hat{n} = (\cos\phi, \sin\phi, 0)$, enabling reversal or completion of the $|G\rangle \leftrightarrow |D\rangle$ transition.

Figure 4(b) shows the steady-state populations as a function of the waiting time τ_c between the last detected jump and the application of a $(\pi/2)$ pulse around the y axis ($\phi = \theta = \pi/2$). For short τ_c, the system remains mostly in $|G\rangle$ after the jump $|B\rangle \to |G\rangle$, so the $(\pi/2)$ pulse transfers population to $|D\rangle$, increasing its steady-state occupation. However, the system may evolve toward $|D\rangle$ before the pulse, which then drives it back to $|G\rangle$, maximizing the $|G\rangle$ population. The inset shows the average interval $\langle\Delta t\rangle$ between photon detections (jumps $|B\rangle \to |G\rangle$) as a function of τ_c. Maximizing P_G enhances coherent excitation to $|B\rangle$, making jumps $|B\rangle \to |G\rangle$ more frequent and reducing $\langle\Delta t\rangle$, while increasing P_D suppresses excitations and lengthens $\langle\Delta t\rangle$. This illustrates how feedback directly shapes the jump statistics, which can also be analyzed in terms of the pulse angles θ and ϕ.

Conclusion—We derived a deterministic equation that describes a general feedback protocol, encompassing both discrete and continuous feedback. It recovers previous results as particular cases, and allows for the derivation of novel feedback schemes, such as time-dependent strategies. Our framework offers numerical efficiency and conceptual clarity through closed-form expressions, allowing analytical identification of operating regimes and critical thresholds—advantages crucial for theory and experiment.

Acknowledgments—The authors acknowledge fruitful discussions with Mark Mitchison, Guilherme Fiusa, and Abhaya Hegde. P. P. P. acknowledges funding from the Swiss National Science Foundation (Eccellenza Professorial Fellowship No. PCEFP2_194268).

Data availability—There are no publicly available research data or software supporting this manuscript. Requests for further information or data should be sent to the authors.

[1] A. Hopkins, K. Jacobs, S. Habib, and K. Schwab, Phys. Rev. B **68**, 235328 (2003).

[2] B. D'Urso, B. Odom, and G. Gabrielse, Phys. Rev. Lett. **90**, 043001 (2003).

[3] D. A. Steck, K. Jacobs, H. Mabuchi, S. Habib, and T. Bhattacharya, Phys. Rev. A **74**, 012322 (2006).

[4] P. Bushev, D. Rotter, A. Wilson, F. m. c. Dubin, C. Becher, J. Eschner, R. Blatt, V. Steixner, P. Rabl, and P. Zoller, Phys. Rev. Lett. **96**, 043003 (2006).

[5] K. Jacobs, H. I. Nurdin, F. W. Strauch, and M. James, Phys. Rev. A **91**, 043812 (2015).

[6] M. Frimmer, J. Gieseler, and L. Novotny, Phys. Rev. Lett. **117**, 163601 (2016).

[7] J. Guo, R. Norte, and S. Gröblacher, Phys. Rev. Lett. **123**, 223602 (2019).

[8] L. Buffoni, A. Solfanelli, P. Verrucchi, A. Cuccoli, and M. Campisi, Phys. Rev. Lett. **122**, 070603 (2019).

[9] S. K. Manikandan and S. Qvarfort, Phys. Rev. A **107**, 023516 (2023).
[10] G. De Sousa, P. Bakhshinezhad, B. Annby-Andersson, P. Samuelsson, P. P. Potts, and C. Jarzynski, Phys. Rev. E **111**, 014152 (2025).
[11] M. Sarovar, C. Ahn, K. Jacobs, and G. J. Milburn, Phys. Rev. A **69**, 052324 (2004).
[12] D. Marcos, A. Smith, A. Bednorz, and N. Yunger Halpern, Phys. Rev. X **10**, 041013 (2020).
[13] D. Ristè, M. Dukalski, C. A. Watson, G. de Lange, M. J. Tiggelman, Y. M. Blanter, K. W. Lehnert, R. N. Schouten, and L. DiCarlo, Nature (London) **502**, 350 (2013).
[14] J. P. Pekola, Nat. Phys. **11**, 118 (2015).
[15] P. P. Potts and P. Samuelsson, Phys. Rev. Lett. **121**, 210603 (2018).
[16] D. Barker, M. Scandi, S. Lehmann, C. Thelander, K. A. Dick, M. Perarnau-Llobet, and V. F. Maisi, Phys. Rev. Lett. **128**, 040602 (2022).
[17] W. G. van der Wiel, S. De Franceschi, J. M. Elzerman, T. Fujisawa, S. Tarucha, and L. P. Kouwenhoven, Rev. Mod. Phys. **75**, 1 (2002).
[18] R. Vijay, C. Macklin, D. H. Slichter, S. J. Weber, K. W. Murch, R. Naik, A. N. Korotkov, and I. Siddiqi, Nature (London) **490**, 77 (2012).
[19] D. Ristè, C. C. Bultink, K. W. Lehnert, and L. DiCarlo, Phys. Rev. Lett. **109**, 240502 (2012).
[20] P. Campagne-Ibarcq, E. Flurin, N. Roch, D. Darson, P. Morfin, M. Mirrahimi, M. H. Devoret, F. Mallet, and B. Huard, Phys. Rev. X **3**, 021008 (2013).
[21] M. T. Mitchison, J. Goold, and J. Prior, Quantum **5**, 500 (2021).
[22] M. D. Vidrighin, O. Dahlsten, M. Barbieri, M. S. Kim, V. Vedral, and I. A. Walmsley, Phys. Rev. Lett. **116**, 050401 (2016).
[23] M. Naghiloo, J. J. Alonso, A. Romito, E. Lutz, and K. W. Murch, Phys. Rev. Lett. **121**, 030604 (2018).
[24] M. Ribezzi-Crivellari and F. Ritort, Nat. Phys. **15**, 660 (2019).
[25] T. Sagawa and M. Ueda, Phys. Rev. Lett. **104**, 090602 (2010).
[26] T. Sagawa and M. Ueda, Phys. Rev. Lett. **109**, 180602 (2012).
[27] K. Funo, Y. Watanabe, and M. Ueda, Phys. Rev. E **88**, 052121 (2013).
[28] A. Tilloy, SciPost Phys. **17**, 083 (2024).
[29] B. Annby-Andersson, F. Bakhshinezhad, D. Bhattacharyya, G. De Sousa, C. Jarzynski, P. Samuelsson, and P. P. Potts, Phys. Rev. Lett. **129**, 050401 (2022).
[30] H. M. Wiseman and G. J. Milburn, Phys. Rev. Lett. **70**, 548 (1993).
[31] H. M. Wiseman, Phys. Rev. A **49**, 2133 (1994).
[32] M. J. Kewming, A. Kiely, S. Campbell, and G. T. Landi, Phys. Rev. A **109**, L050202 (2024).
[33] K. Jacobs and D. A. Steck, Contemp. Phys. **47**, 279 (2006).
[34] H. M. Wiseman and G. J. Milburn, *Quantum Measurement and Control* (Cambridge University Press, Cambridge, England, 2010).
[35] V. P. Belavkin, Autom. Remote Control (English Translation) **44**, 178 (1983).
[36] V. P. Belavkin, J. Multivariate Anal. **42**, 171 (1992).
[37] V. P. Belavkin, in *Information Complexity and Control in Quantum Physics*, edited by A. Blaquiere, S. Diner, and G. Lochak (Springer, Vienna, 1987), pp. 311–329.
[38] V. P. Belavkin, Commun. Math. Phys. **146**, 611 (1992).
[39] A. N. Korotkov, Phys. Rev. B **63**, 115403 (2001).
[40] K. Jacobs, *Quantum Measurement Theory and its Applications* (Cambridge University Press, Cambridge, England, 2014).
[41] J. Zhang, Y.-X. Liu, R.-B. Wu, K. Jacobs, and F. Nori, Phys. Rep. **679**, 1 (2017).
[42] C. Sayrin, I. Dotsenko, X. Zhou, B. Peaudecerf, T. Rybarczyk, S. Gleyzes, P. Rouchon, M. Mirrahimi, H. Amini, M. Brune, J.-M. Raimond, and S. Haroche, Nature (London) **477**, 73 (2011).
[43] Z. K. Minev, S. O. Mundhada, S. Shankar, P. Reinhold, R. Gutiérrez-Jáuregui, R. J. Schoelkopf, M. Mirrahimi, H. J. Carmichael, and M. H. Devoret, Nature (London) **570**, 200 (2019).
[44] A. Hofmann, V. F. Maisi, C. Gold, T. Krähenmann, C. Rössler, J. Basset, P. Märki, C. Reichl, W. Wegscheider, K. Ensslin, and T. Ihn, Phys. Rev. Lett. **117**, 206803 (2016).
[45] F. Ye, A. Ellaboudy, and J. M. Nichol, Phys. Rev. Appl. **23**, 044063 (2025).
[46] It turns out that if the system is incoherent, this example can be described using classical master equations [47], but this is no longer possible in a genuinely coherent scenario.
[47] B. Annby-Andersson, P. Samuelsson, V. F. Maisi, and P. P. Potts, Phys. Rev. B **101**, 165404 (2020).
[48] See Supplemental Material at http://link.aps.org/supplemental/10.1103/pg2p-h529 for detailed derivations of the main results and the examples presented in this Letter.
[49] A. J. B. Rosal, P. P. Potts, and G. T. Landi, companion article, Phys. Rev. A **114**, 012215 (2026).
[50] A. J. B. Rosal, G. Fiusa, P. P. Potts, and G. T. Landi, companion article, Phys. Rev. A **114**, 012216 (2026).
[51] The continuous monitoring limit is obtained by applying measurements at regular intervals $t_i = i\delta t$ with $\delta t > 0$, and then taking the limit $\delta t \to 0$.
[52] S. Milz and K. Modi, PRX Quantum **2**, 030201 (2021).
[53] I. Layton, J. Oppenheim, and Z. Weller-Davies, Quantum **8**, 1565 (2024).
[54] L. Diósi, Phys. Rev. A **107**, 062206 (2023).
[55] J. Oppenheim, C. Sparaciari, B. Šoda, and Z. Weller-Davies, Quantum **7**, 891 (2023).
[56] J. Oppenheim, Phys. Rev. X **13**, 041040 (2023).
[57] G. T. Landi, M. J. Kewming, M. T. Mitchison, and P. P. Potts, PRX Quantum **5**, 020201 (2024).
[58] P. Blanchard and A. Jadczyk, Ann. Phys. (Berlin) **507**, 583 (1995).
[59] M. Hofheinz, E. M. Weig, M. Ansmann, R. C. Bialczak, E. Lucero, M. Neeley, A. D. O'Connell, H. Wang, J. M. Martinis, and A. N. Cleland, Nature (London) **454**, 310 (2008).
[60] N. Maring *et al.*, Nat. Photonics **18**, 603 (2024).
[61] J. C. Bergquist, R. G. Hulet, W. M. Itano, and D. J. Wineland, Phys. Rev. Lett. **57**, 1699 (1986).
[62] T. Sauter, W. Neuhauser, R. Blatt, and P. E. Toschek, Phys. Rev. Lett. **57**, 1696 (1986).
[63] W. Nagourney, J. Sandberg, and H. Dehmelt, Phys. Rev. Lett. **56**, 2797 (1986).
[64] R. J. Cook and H. J. Kimble, Phys. Rev. Lett. **54**, 1023 (1985).

End Matter

Appendix A: Population inversion protocol—The feedback protocol considered in Example 1 affects only the system's Hamiltonian; hence, the steady state can be obtained from Eq. (13). A detailed derivation is provided in Supplemental Material [48], which gives the analytical expression for the excited-state population $P_e = \langle e|\rho_{ss}|e\rangle$ at resonance ($\Delta = 0$) as a function of the bath parameters $\bar{N}$ and γ, and the feedback parameters λ, τ_0, and τ_1. By maximizing P_e with respect to τ_1, one obtains the optimal duration τ_1^{opt} for which the external drive should remain on. We find that

$$\tau_1^{\mathrm{opt}} = \frac{2\left[2\pi + \arctan\left(\frac{p\sqrt{16-p^2}}{8-p^2}\right) - \pi\theta(\sqrt{8}-p)\right]}{\lambda\sqrt{16-p^2}}, \tag{A1}$$

where $p = \gamma/\lambda$ and $\theta(x)$ is the Heaviside function. This is finite only for $p < 4$, and diverges otherwise. It is noteworthy that τ_1^{opt} is independent of both the feedback delay τ_0 and the bath occupation $\bar{N}$; it depends solely on the ratio $p = \gamma/\lambda$ between the coupling rate to the bath and the drive strength.

Next we consider a more realistic scenario where we have a time delay τ_0 between the last detected jump and the moment the external drive is turned on. Even in this more general case, the optimal drive duration that maximizes the population of the excited state remains given by Eq. (A1) [48]. In the low-temperature limit $\bar{N} \to 0$, the expression for P_e, evaluated at the optimal drive duration, simplifies to

$$\lim_{\bar{N}\to 0} P_e = \frac{1}{2 - e^{-\gamma\tau_1^{\mathrm{opt}}/2} + \frac{1}{4}\left(\frac{\gamma}{\lambda}\right)^2 + \gamma\tau_0}. \tag{A2}$$

In the limit $\bar{N} \to 0$, population inversion ($P_e > 1/2$) occurs only for time delays below a maximum value $\tau_0^{\max}$, given by

$$\tau_0^{\max} = \frac{4e^{-\gamma\tau_1^{\mathrm{opt}}/2} - (\gamma/\lambda)^2}{4\gamma}. \tag{A3}$$

It is worth mentioning that this protocol can be adapted to increase the population of the ground state: by turning on the drive when an absorption is detected, the drive will move the system toward the ground state through Rabi oscillations. In this case, the protocol effectively operates as a cooling protocol based on quantum jump detections.

Appendix B: Reverting quantum transitions—Reference [43] experimentally implemented the feedback protocol described in Example 2. Instead of directly monitoring the incoherent jump $|B\rangle \to |G\rangle$ via photon detection, they coupled the bright state $|B\rangle$ to a readout cavity. The population of $|B\rangle$ was then inferred by measuring the number of photons in the cavity, allowing them to determine whether the system was in $|B\rangle$ or in a superposition of $|G\rangle$ and $|D\rangle$. However, as discussed in Supplemental Material of Ref. [43], a photon-counting scheme (as adopted in Example 2) can serve as a first approximation to the experimental results obtained via indirect monitoring of $|B\rangle$ using homodyne detection in the cavity. The authors' theoretical description employed

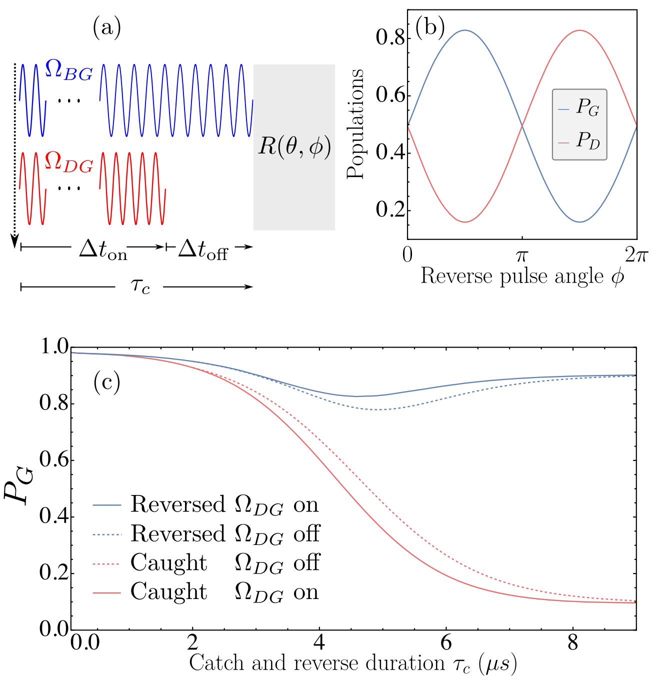

FIG. 5. Populations of the system's state immediately after the pulse. (a) The vertical arrow on the left-hand side represents the last detected jump $|B\rangle \to |G\rangle$, and the horizontal axis indicates the time elapsed since its detection. The system is driven by Ω_{BG} (blue line) and Ω_{DG} (red line). After a time τ_c has elapsed since the last jump, a pulse $R(\theta,\phi)$ is applied in the $\{|G\rangle, |D\rangle\}$ subspace. The drive Ω_{DG} can either remain on during the full interval τ_c or be turned off after a time Δt_{on}. (b) Populations of the ground $|G\rangle$ (P_G) and dark $|D\rangle$ (P_D) states after the pulse for $\theta = \pi/2$, as a function of the direction angle ϕ, for $\tau_c = 4.2$ μs. (c) Population P_G of the ground state as a function of the waiting time τ_c. Solid lines correspond to the case where the drive Ω_{DG} remains on during τ_c, while dashed lines correspond to the case where Ω_{DG} is turned off after a time Δt_{on}, as illustrated in (a). Blue curves represent the feedback case (rotation applied), while red curves correspond to the no-feedback case (no rotation after τ_c). In the feedback case, for each τ_c we determine the optimal pulse angles $\{\theta(\tau_c), \phi(\tau_c)\}$ that maximize P_G, and use them to compute $P_G(\tau_c)$. The parameters $\gamma_{B,D}$, $\bar{N}_{B,D}$, Ω_{BG}, and Ω_{DG} are the same as those used in Fig. 4.

stochastic equations accounting for the random homodyne signal, which were used to sample system trajectories conditioned on a given homodyne measurement.

A photon-counting scheme can be implemented by monitoring intermittent fluorescence from the bright state $|B\rangle$ in trapped ions [61–64]. This scheme tracks the incoherent jumps $|B\rangle \to |G\rangle$, and our formalism directly provides the steady state of this feedback protocol as the solution of an eigenvector problem, as well as the jump statistics in the stationary regime. The feedback protocol in Example 2 does not modify the jump operators; the feedback action consists of applying a pulse in the $\{|G\rangle, |D\rangle\}$ subspace after a time τ_c has elapsed since the last detected jump. Consequently, the steady state is given by Eq. (13) (see Supplemental Material [48] for details).

Our framework provides the analytical solution of the system state immediately after the pulse, as reported in Fig. 4 of Ref. [43]. The populations of this conditioned state, considering the photon-counting scheme of Example 2, are shown in Fig. 5. From our formalism (see Ref. [48]), the state immediately after the pulse, assuming Ω_{DG} is continuously on, reads

$$\rho_{\rm on}(\tau_c) = \frac{R(\theta,\phi)e^{\tau_c \mathcal{L}_0^{(1)}}(|G\rangle\langle G|)}{\mathrm{Tr}[R(\theta,\phi)e^{\tau_c \mathcal{L}_0^{(1)}}(|G\rangle\langle G|)]}, \tag{B1}$$

where $\mathcal{L}_0^{(1)}$ is the no-jump Liouvillian with both drives Ω_{DG} and Ω_{BG} active during τ_c [see Fig. 5(a)], and $R(\theta, \phi)$ represents the rotation in the $\{|G\rangle, |D\rangle\}$ subspace. In Example 2, we keep Ω_{DG} on continuously for simplicity, but we can also consider turning it off after a time $\Delta t_{\rm on}$ since the last jump, keeping only Ω_{BG} active, as illustrated in Fig. 5(a). In this case, the state immediately after the pulse reads

$$\rho_{\rm off}(\tau_c) = \frac{R(\theta,\phi)e^{\Delta t_{\rm off}\mathcal{L}_0^{(2)}}e^{\Delta t_{\rm on}\mathcal{L}_0^{(1)}}(|G\rangle\langle G|)}{\mathrm{Tr}[R(\theta,\phi)e^{\Delta t_{\rm off}\mathcal{L}_0^{(2)}}e^{\Delta t_{\rm on}\mathcal{L}_0^{(1)}}(|G\rangle\langle G|)]}, \tag{B2}$$

where $\mathcal{L}_0^{(2)}$ is the no-jump Liouvillian with only Ω_{BG} active.

The interpretation of Eqs. (B1) and (B2) is straightforward: since the jump $|B\rangle \to |G\rangle$ is a renewal process [57], the system resets to $|G\rangle$ after each jump. If no jump occurs during the interval τ_c, the system evolves under the appropriate no-jump Liouvillian, after which the rotation $R(\theta, \phi)$ is applied. Both Eqs. (B1) and (B2) follow directly from the memory-resolved steady state $\varrho_{ss}(k, \tau)$ in Result 2, representing the system state given a time τ_c since the last jump. For Example 2, only the jump $|B\rangle \to |G\rangle$ is monitored, so the memory-resolved state depends solely on τ, denoted by $\varrho_{ss}(\tau)$.

The memory-resolved steady state reads

$$\varrho_{ss}(\tau) = \gamma_B(\bar{N}_B + 1)\langle B|\bar{\rho}_{ss}|B\rangle G(\tau)(|G\rangle\langle G|), \tag{B3}$$

where $G(\tau)$ is the no-jump propagator and $\bar{\rho}_{ss}$ is the unconditional steady state given by Eq. (13). For Ω_{DG} always on, $G(\tau)$ is

$$G(\tau) = \begin{cases} e^{\tau\mathcal{L}_0^{(1)}}, & \text{if } \tau < \tau_c, \\ e^{(\tau-\tau_c)\mathcal{L}_0^{(1)}}R(\theta,\phi)e^{\tau_c\mathcal{L}_0^{(1)}}, & \text{if } \tau \geq \tau_c. \end{cases} \tag{B4}$$

The trace $\mathrm{Tr}[\varrho_{ss}(\tau)]$ gives the stationary probability density of detecting a jump and observing no-jump evolution for a time τ. This provides the jump statistics under feedback, showing how the protocol systematically shapes the jumps and directly connecting to measurable quantities.